A Unified Hybrid-Mode Analysis for Planar Transmission Lines with Multilayer Isotropic/Anisotropic Substrates

RAAFAT R. MANSOUR, MEMBER, IEEE, AND ROBERT H. MACPHIE, SENIOR MEMBER, IEEE

Abstract—**A unified hybrid-mode analysis is presented for determining the propagation characteristics of multiconductor, multilayer planar transmission lines. The analysis employs the conservation of complex power technique, and the emphasis is on numerical efficiency and simplicity. Numerical results, for finline and microstrip configurations, aim at the clarification of the effects of the metalization thickness, dielectric anisotropy, and substrate mounting grooves.**

I. INTRODUCTION

DURING THE PAST several years, a variety of techniques have been published for the characterization of planar transmission lines, techniques wherein there has been always a compromise between accuracy and numerical efficiency. In many cases, simplified approximations were introduced to achieve a good numerical efficiency at the expense of the accuracy. For example, most published techniques do not take into account the effect of the substrate mounting groove. Elsewhere numerous results are reported for idealized structures with zero metallization thickness.

With the increasing complexity of microwave and millimeter-wave circuit design, attention has been directed in recent years to generalized approaches that can treat a variety of planar transmission lines with more complicated configurations. Thus, in developing a new technique the "generalization" has become another challenging factor to be considered in addition to the accuracy and numerical efficiency.

Among the published rigorous techniques for analyzing planar transmission lines are the spectral-domain technique and the singular integral equation technique [1], [2]. Although these techniques have a very good numerical efficiency, they do not include the effects of metallization thickness and substrate mounting grooves. The metallization thickness has been taken into account by Beyer [3] and Vahldieck [4] using the mode-matching technique, and also by Kitazawa and Mittra [5] using the network analytical method. The effect of mounting grooves has been considered as well in [3] and [4], but these methods were presented to treat only finline structures. The effect of the metallization thickness on the propagation characteristics of multiconductor planar transmission lines has been approximately taken into account by Saad and Schunemann [6]. However, the approximation involved in this method is only valid for structures with large slot widths.

Very recently, an approach based on the mode-matching technique has been presented by Vahldieck and Bornemann in [7] to calculate the propagation constant, and extended by Bornemann and Arndt in [8] to calculate the characteristic impedance. However, as will be shown in Section II, this approach has a very poor numerical efficiency. Moreover, in view of the study given in [9] on the convergence of the modal analysis numerical solution, the mode-matching formulation used in this approach suffers from serious convergence problems and may fail to provide accurate results for structures with relatively small metallization thickness.

In this contribution, we present the details of a hybrid-mode approach for evaluating the propagation constants of the dominant and the higher order modes and the characteristic impedance for planar transmission lines with multiconductor and multilayer isotropic/anisotropic substrates. Besides the versatility and flexibility of this approach in treating complicated structures, it is numerically efficient and it includes the effects of the metallization thickness and substrate mounting grooves.

II. FORMULATION OF THE PROBLEM

A generalized planar guiding structure is shown in Fig. 1. It consists of an arbitrary number of metallic strips deposited on various interfaces of a multilayer isotropic/anisotropic dielectric substrate. The hybrid nature of the electromagnetic field in this structure can be attributed to the coupling between LSE and LSM modes. By considering the propagation to take place along the transverse direction, the discontinuities at the various vertical planes serve to couple the LSE and LSM modes, and the hybrid modes are formed as a result of the repeated reflections of LSE and LSM modes from the short-circuited ends and the discontinuities.

Manuscript received April 2, 1987; revised August 17, 1987. This work was supported in part by the Natural Sciences and Engineering Research Council, Ottawa, Canada, under Grant A-2176.

R. R. Mansour is with COM DEV Ltd., Cambridge, Ontario, Canada NIR 7H6.

R. H. MacPhie is with the Department of Electrical Engineering, University of Waterloo, Waterloo, Ontario, Canada N2L 3G1.

IEEE Log Number 8717395.

0018-9480/87/1200-1382$01.00 ©1987 IEEE

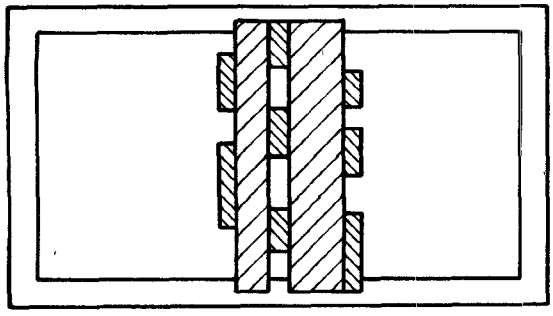

Fig. 1. A generalized planar guiding structure.

The first step in the analysis uses the conservation of complex power technique (CCPT) to treat the problem of scattering at the N-furcated waveguide discontinuity shown in Fig. 2 for LSE and LSM excitation. The LSE and LSM modes may be derived from magnetic- and electric-type Hertzian potential functions [10] having single components directed normal to the xz plane. The appropriate solutions for $\vec{\Pi}^h_{in}$ and $\vec{\Pi}^e_{in}$ in the ith guide are given by

$$\vec{\Pi}^h_{in} = \frac{1}{j\omega\mu K_{c,in}} \cos\frac{n\pi}{L_i} x\, e^{-j\alpha^h_{in} y}\, e^{-j\beta z} a_y \tag{1}$$

$$\vec{\Pi}^e_{in} = \frac{1}{j\alpha_{in} K_{c,in}} \sin\frac{n\pi}{L_i} x\, e^{-j\alpha^e_{in} y}\, e^{-j\beta z} \vec{a}_y. \tag{2}$$

The propagation constant along the z direction is represented by the exponential factor $e^{-j\beta z}$ and assumed to be the same in all guides and for both LSE and LSM modes. The transverse components of the fields may then given by

$$\vec{e}^h_{in} = \frac{1}{K_{c,in}}\left[-j\beta\cos\frac{n\pi}{L_i}x\,\vec{a}_x + \frac{n\pi}{L_i}\sin\frac{n\pi}{L_i}x\,\vec{a}_z\right] e^{-j\alpha^h_{in}y} e^{-j\beta z} \tag{3a}$$

$$\vec{h}^h_{in} = \frac{Y^h_{in}}{K_{c,in}}\left[+\frac{n\pi}{L_i}\sin\frac{n\pi}{L_i}x\,\vec{a}_x + j\beta\cos\frac{n\pi}{L_i}x\,\vec{a}_z\right] e^{-j\alpha^h_{in}y} e^{-j\beta z} \tag{3b}$$

$$\vec{e}^e_{in} = \frac{1}{K_{c,in}}\left[-\frac{n\pi}{L_i}\cos\frac{n\pi}{L_i}x\,\vec{a}_x + j\beta\sin\frac{n\pi}{L_i}x\,\vec{a}_z\right] e^{-j\alpha^e_{in}y} e^{-j\beta z} \tag{3c}$$

$$\vec{h}^e_{in} = \frac{Y^e_{in}}{K_{c,in}}\left[+j\beta\sin\frac{n\pi}{L_i}x\,\vec{a}_x + \frac{n\pi}{L_i}\cos\frac{n\pi}{L_i}x\,\vec{a}_z\right] e^{-j\alpha^e_{in}y} e^{-j\beta z} \tag{3d}$$

where

$$\alpha^h_{in} = \alpha^e_{in} = \left[\omega^2\mu\epsilon_i - \left(\frac{n\pi}{L_i}\right)^2 - \beta^2\right]^{1/2}$$

$$K_{c,in} = \left[\left(\frac{n\pi}{L_i}\right)^2 + \beta^2\right]^{1/2},$$

$n = 0,1,2,\cdots$ for LSE

$n = 1,2,3,\cdots$ for LSM

$$Y^h_{in} = \frac{\alpha^h_{in}}{\omega\mu} \qquad Y^e_{in} = \frac{\omega\epsilon}{\alpha^e_{in}} \qquad \text{(modal admittances)}.$$

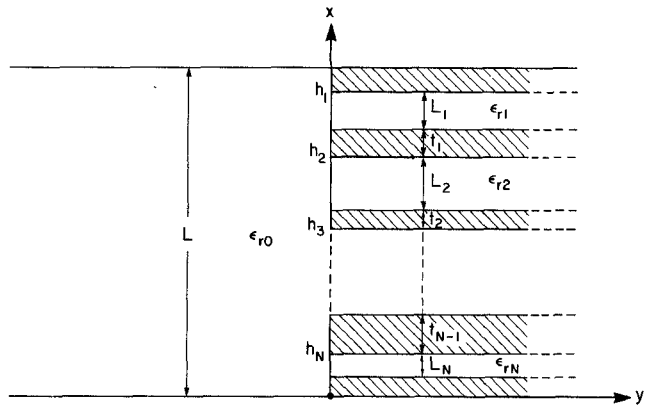

Fig. 2. An N-furcated waveguide junction.

Let the transverse fields in the ith guide at $y = 0$, $z = 0$ be represented[1] by an infinite sum of LSE-mode electric fields $\vec{e}^h_{in}$ and LSM-mode electric fields $\vec{e}^e_{in}$:

$$\vec{E}_i(x) = \sum_{n=0,1,2,\cdots} A^h_{in}\vec{e}^h_{in}(x) + \sum_{n=1,2,3,\cdots} A^e_{in}\vec{e}^e_{in}(x) \tag{4}$$

where A^h_{in} and A^e_{in} are the nth LSE- and LSM-mode amplitudes respectively in the ith guide, $i = 0,1,2,\ldots,N$. Because of the coupling between the LSE and LSM modes, the three basic matrices $\boldsymbol{H}$, $\boldsymbol{P}_A$, and $\boldsymbol{P}_B$ defined in the CCPT formulation [11] can be written

$$\begin{bmatrix}\underline{A}^h_0\\ \underline{A}^e_0\end{bmatrix} = \begin{bmatrix}\boldsymbol{H}^{hh}_1 & \boldsymbol{H}^{he}_1 & \boldsymbol{H}^{hh}_2 & \cdots & \boldsymbol{H}^{hh}_N & \boldsymbol{H}^{he}_N\\ \boldsymbol{H}^{eh}_1 & \boldsymbol{H}^{ee}_1 & \boldsymbol{H}^{eh}_2 & \cdots & \boldsymbol{H}^{eh}_N & \boldsymbol{H}^{ee}_N\end{bmatrix}\begin{bmatrix}\underline{A}^h_1\\ \underline{A}^e_1\\ \underline{A}^h_2\\ \vdots\\ \underline{A}^h_N\\ \underline{A}^e_N\end{bmatrix} \tag{5}$$

$$\boldsymbol{H} = \begin{bmatrix}\boldsymbol{H}^{hh}_1 & \boldsymbol{H}^{he}_1 & \boldsymbol{H}^{hh}_2 & \cdots & \boldsymbol{H}^{hh}_N & \boldsymbol{H}^{he}_N\\ \boldsymbol{H}^{eh}_1 & \boldsymbol{H}^{ee}_1 & \boldsymbol{H}^{eh}_2 & \cdots & \boldsymbol{H}^{eh}_N & \boldsymbol{H}^{ee}_N\end{bmatrix} \tag{6}$$

$$\boldsymbol{P}_A = \begin{bmatrix}\boldsymbol{P}^h_A & \boldsymbol{0}\\ \boldsymbol{0} & \boldsymbol{P}^e_A\end{bmatrix} \tag{7a}$$

$$\boldsymbol{P}_B = \begin{bmatrix}\boldsymbol{P}^h_{B1} & 0 & 0 & \cdots & 0 & 0\\ 0 & \boldsymbol{P}^e_{B1} & 0 & \cdots & 0 & 0\\ 0 & 0 & \boldsymbol{P}^h_{B2} & \cdots & 0 & 0\\ \vdots & \vdots & \vdots & \cdots & \vdots & \vdots\\ 0 & 0 & 0 & \cdots & \boldsymbol{P}^h_{BN} & 0\\ 0 & 0 & 0 & \cdots & 0 & \boldsymbol{P}^e_{BN}\end{bmatrix}. \tag{7b}$$

where h and e refer to LSE and LSM modes, respectively. $\boldsymbol{H}$ is the E-field mode-matching matrix which represents the coupling between the modes in the large guide and

[1] From now on we will use the following notations: † denotes Hermitian transpose; * denotes complex conjugate. All column matrices are denoted with an underbar, and all matrices are in boldface.

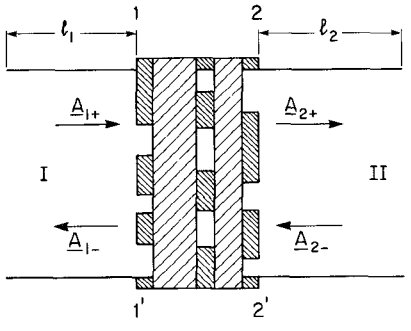

Fig. 3. A generalized discontinuity

those of the N-furcated guide. $\boldsymbol{P}_A^h$, $\boldsymbol{P}_A^e$, $\boldsymbol{P}_{Bi}^h$, and $\boldsymbol{P}_{Bi}^e$ for $i=1,2,3,\ldots,N$, are diagonal matrices with diagonal elements representing the powers carried by unit amplitude LSE and LSM modes in the various guides. If (P LSE + P LSM) modes are retained in the large guide whereas (Q LSE + Q LSM) modes are retained in the N-furcated guide, the size of the matrices $\boldsymbol{H}$, $\boldsymbol{P}_A$, and $\boldsymbol{P}_B$ are respectively $(2P\times 2Q)$, $(2P\times 2P)$, and $(2Q\times 2Q)$.

The cross-coupling between LSE and LSM modes is readily understood from (5). However, it is interesting to note that if we let $\beta=0$, all the elements of the matrices $\boldsymbol{H}_i^{eh}$ and $\boldsymbol{H}_i^{he}$ for $i=1,2,\ldots,N$, would vanish. In this case the LSE and LSM modes become TE and TM modes, respectively, with a direction of propagation normal to the xz plane. As has been seen in [11], these modes are not coupled by scattering at N-furcated parallel-plate waveguide junctions.

In view of [9] and after some manipulations, the transmission matrix of the N-furcated discontinuity can be determined in terms of the three basic matrices $\boldsymbol{H}$, $\boldsymbol{P}_A$, and $\boldsymbol{P}_B$ derived above for LSE and LSM excitation. The transmission matrix $\boldsymbol{T}^T$ of the overall discontinuity shown in Fig. 3 can then be easily obtained by simple matrix multiplications.

The next step is to apply the transverse resonance technique to find the eigenvalue equation for the propagation constant β. Let the parameters of the overall transmission matrix $\boldsymbol{T}^T$ be written as

$$\underline{A}_{1+}=\boldsymbol{T}_{11}^T\,\underline{A}_{2+}+\boldsymbol{T}_{12}^T\,\underline{A}_{2-} \tag{8a}$$

$$\underline{A}_{1-}=\boldsymbol{T}_{21}^T\,\underline{A}_{2+}+\boldsymbol{T}_{22}^T\,\underline{A}_{2-} \tag{8b}$$

where $\underline{A}_{i+}$ ($\underline{A}_{i-}$), $i=1,2$, are the forward (backward) LSE and LSM mode vectors at planes $11',22'$, as indicated in Fig. 3. These mode vectors are also related as follows:

$$\underline{A}_{1+}=-\boldsymbol{L}_1^-\boldsymbol{L}_1^-\underline{A}_{1-}\qquad \underline{A}_{2-}=-\boldsymbol{L}_2^-\boldsymbol{L}_2^-\underline{A}_{2+} \tag{9a}$$

where

$$\boldsymbol{L}_1^-=\begin{bmatrix}\boldsymbol{L}_1^{-h} & \boldsymbol{0}\\ \boldsymbol{0} & \boldsymbol{L}_1^{-e}\end{bmatrix}\qquad \boldsymbol{L}_2^-=\begin{bmatrix}\boldsymbol{L}_2^{-h} & \boldsymbol{0}\\ \boldsymbol{0} & \boldsymbol{L}_2^{-e}\end{bmatrix}. \tag{9b}$$

$\boldsymbol{L}_1^{-h}$, $\boldsymbol{L}_1^{-e}$, $\boldsymbol{L}_2^{-h}$, and $\boldsymbol{L}_2^{-e}$ are diagonal matrices with diagonal elements given by

$$L_{1,nn}^{-h}=L_{1,nn}^{-e}=e^{-j[\omega^2\mu\epsilon-(n\pi/L)^2-\beta^2]^{1/2}l_1} \tag{10a}$$

$$L_{2,nn}^{-h}=L_{2,nn}^{-e}=e^{-j[\omega^2\mu\epsilon-(n\pi/L)^2-\beta^2]^{1/2}l_2} \tag{10b}$$

$n=0,1,2,\ldots,Q$ for LSE modes

$n=1,2,3,\ldots,Q$ for LSM modes.

In (10), l_1 and l_2 are, respectively, the lengths of the waveguide sections I and II shown in Fig. 3. Manipulating (8) and (9) gives

$$\begin{bmatrix}\boldsymbol{I} & -\left[\boldsymbol{T}_{11}^T-\boldsymbol{T}_{12}^T\boldsymbol{L}_2^-\boldsymbol{L}_2^-\right]\\ \boldsymbol{I} & \boldsymbol{L}_1^-\boldsymbol{L}_1^-\left[\boldsymbol{T}_{21}^T-\boldsymbol{T}_{22}^T\boldsymbol{L}_2^-\boldsymbol{L}_2^-\right]\end{bmatrix}\begin{bmatrix}\underline{A}_{1+}\\ \underline{A}_{2+}\end{bmatrix}=\boldsymbol{0}. \tag{11}$$

For a nontrivial solution the determinant should vanish:

$$\mathrm{Det}\left[\boldsymbol{L}_1^-\boldsymbol{L}_1^-\left[\boldsymbol{T}_{21}^T-\boldsymbol{T}_{22}^T\boldsymbol{L}_2^-\boldsymbol{L}_2^-\right]+\left[\boldsymbol{T}_{11}^T-\boldsymbol{T}_{12}^T\boldsymbol{L}_2^-\boldsymbol{L}_2^-\right]\right]=0. \tag{12}$$

The solution for the propagation constant β may then be determined by seeking the zeros of the above determinantal equation.

The size of the eigenvalue matrix given in (12) is $(2Q\times 2Q)$, where $2Q$ is the number of modes (LSE + LSM) used in the N-furcated section, which is, in most practical configurations, much less than the number of modes $2P$ originally retained in the large guide to satisfy the edge condition. Since in the waveguide sections I and II indicated in Fig. 3, all the higher order modes are usually below cutoff, the elements associated with these modes in the matrices $\boldsymbol{L}_1^-$ and $\boldsymbol{L}_2^-$ are very small. Thus only the first few modes are needed in the application of the transverse resonance technique and a size of $(2Q\times 2Q)$ for the eigenvalue matrix is quite enough to provide accurate results for most practical applications.

In order to compare the numerical efficiency of the formulation presented in this paper to that reported in [7] and [8], let us consider as an example a typical unilateral finline structure with $d/b=0.2$, where d is the slot width and b is the waveguide height. Let us also assume that $P=25$ and $Q=5$, i.e., (25 LSE modes + 25 LSM modes) are retained in the large guide, and (5 LSE modes + 5 LSM modes) are retained in the slot region. To avoid the relative convergence problem, it is noted that these numbers of modes are chosen such that $P/Q=b/d$. Thus, the size of the eigenvalue matrix derived in our formulation is only (10×10). On the other hand, as stated in [7], with 25 summation terms in the large waveguide (25 TE modes + 25 TM modes) the formulation handles transmission matrices of size (100×100) and leads to an eigenvalue equation of matrix size (50×50).

The considerable reduction of the matrix size we have achieved here is attributed to the use of the improved transmission matrix formulation for cascaded discontinuities, which has been introduced in [9]. This formulation does *not require the use of an equal number of modes*, which makes it possible to impose the edge condition and consequently guarantees accurate evaluation of the trans-

mission parameters. Moreover it makes it possible to derive an eigenvalue matrix of size $(2Q \times 2Q)$ rather than $(2P \times 2P)$.

III. The Characteristic Impedance

With the eigenvalue β calculated, solving the eigenvalue equation for the eigenvector gives the field amplitudes in the various regions which are needed in the calculation of the characteristic impedance. There has been a considerable interest over the past several years in the theoretical investigation of the impedance. Most published results, however, are for structures with zero metallization thickness and no mounting grooves. In this contribution the effects of these parameters on the characteristic impedance based on the voltage–power definition will be investigated.

$$Z = \frac{VV^*}{2P} \qquad P = \sum_i P_i \tag{13}$$

where V is the slot voltage, which is obtained by line integrating the electric field over the width of the appropriate slot; the summation is on all guides involved and P_i is the power flow in guide i:

$$P_i = \frac{1}{2} \operatorname{Re} \int \vec{E}_i \times \vec{H}_i^* \cdot \vec{a}_z \, ds. \tag{14}$$

$\vec{E}_i$ and $\vec{H}_i$ are, respectively, the transverse components (with respect to z) of the electric and magnetic fields in the ith guide:

$$\vec{E}_i = \sum_{n=0,1,2,\cdots} \vec{\phi}_{in}^{\,h} + \sum_{n=1,2,3,\cdots} \vec{\phi}_{in}^{\,e} \tag{15}$$

$$\vec{H}_i = \sum_{n=0,1,2,\cdots} \vec{\psi}_{in}^{\,h} + \sum_{n=1,2,3,\cdots} \vec{\psi}_{in}^{\,e} \tag{16}$$

where

$$\vec{\phi}_{in}^{\,h} = \frac{-j\beta}{K_{c,in}} \cos \frac{n\pi}{L_i} x \, Q_{in}^h \, \vec{a}_x \tag{17a}$$

$$\vec{\psi}_{in}^{\,h} = \frac{Y_{in}^h}{K_{c,in}} \frac{n\pi}{L_i} \sin \frac{n\pi}{L_i} x \, W_{in}^h \, \vec{a}_x + \frac{K_{c,in}}{j\omega\mu} \cos \frac{n\pi}{L_i} x \, Q_{in}^h \, \vec{a}_y \tag{17b}$$

$$\vec{\phi}_{in}^{\,e} = \frac{-1}{K_{c,in}} \frac{n\pi}{L_i} \cos \frac{n\pi}{L_i} x \, Q_{in}^e \, \vec{a}_x + \frac{K_{c,in}}{j\alpha_{in}^e} \sin \frac{n\pi}{L_i} x \, W_{in}^e \, \vec{a}_y \tag{17c}$$

$$\vec{\psi}_{in}^{\,e} = \frac{jY_{in}^e \beta}{K_{c,in}} \sin \frac{n\pi}{L_i} x \, W_{in}^e \, \vec{a}_x. \tag{17d}$$

Q_{in}^h, W_{in}^h, Q_{in}^e, and W_{in}^e are scalar functions given by

$$Q_{in}^h = A_{in+}^h e^{-j\alpha_{in}^h y} + A_{in-}^h e^{+j\alpha_{in}^h y} \tag{18a}$$

$$W_{in}^h = A_{in+}^h e^{-j\alpha_{in}^h y} - A_{in-}^h e^{+j\alpha_{in}^h y} \tag{18b}$$

$$Q_{in}^e = A_{in+}^e e^{-j\alpha_{in}^e y} + A_{in-}^e e^{+j\alpha_{in}^e y} \tag{18c}$$

$$W_{in}^e = A_{in+}^e e^{-j\alpha_{in}^e y} - A_{in-}^e e^{+j\alpha_{in}^e y}. \tag{18d}$$

A_{in+}, A_{in-} denote, respectively, the amplitude of the incident and the reflected nth mode in guide i. Substituting (15)–(18) into (14) gives

$$P_i = P_i^{hh} + P_i^{ee} + P_i^{eh} \tag{19}$$

where

$$P_i^{hh} = \sum_{n=0,1,2,\cdots} \frac{\beta L_i}{4\omega\mu} \Gamma_n \int_0^{l_i} Q_{in}^h Q_{in}^{*h} \, dy \tag{20}$$

$$P_i^{ee} = \sum_{n=1,2,\cdots} \frac{\omega\epsilon\beta L_i}{4\alpha_{in}^e \alpha_{in}^{*e}} \int_0^{l_i} W_{in}^e W_{in}^{*e} \, dy \tag{21}$$

$$P_i^{eh} = \sum_{n=1,2,\cdots} \frac{-jL_i}{4\omega\mu} \frac{n\pi}{L_i} \int_0^{l_i} Q_{in}^e Q_{in}^{*h} \, dy + \frac{j\alpha_{in}^{*h} L_i}{4\omega\mu\alpha_{in}^e} \frac{n\pi}{L_i} \int_0^{l_i} W_{in}^e W_{in}^{*h} \, dy. \tag{22}$$

In (20) $\Gamma_n = 2$ for $n = 0$ and $\Gamma_n = 1$ for $n = 1, 2, \cdots$.

Originally, it was assumed that $2P$ modes were retained in the large guide and $2Q$ modes were retained in the N-furcated guide. The solution of the eigenvalue equation will provide, however, only information about the amplitudes of $2Q$ modes in all guides. Although a matrix size of $(2Q \times 2Q)$ for the eigenvalue equation is usually enough to achieve good results for the propagation constant β, in calculating the power flow, $2Q$ modes may not be sufficient to accurately represent the total power propagating in the large guide.

Indeed, investigation of the convergence of the calculated results showed that accurate calculation of the power flow requires the use of more modes in the large guide. The coefficients of those additional modes can be deduced *without increasing the size of the eigenvalue matrix*. This additional information is obtained from the E-field mode-matching matrix $\boldsymbol{H}$, which has a size of $(2P \times 2Q)$ and has been derived at the beginning of the formulation.

IV. Planar Transmission Lines on Anisotropic Substrates

The problem of analyzing planar transmission lines on anisotropic substrates has been studied by many investigators using quasi-static as well as hybrid-mode analyses. Recently, a comprehensive review entitled "Integrated-Circuit Structures on Anisotropic Substrates" has been published by Alexopoulos [12]. This paper discusses in detail the different techniques used in analyzing these structures and contains an exhaustive list of references to the existing literature. It is noted, however, that the great majority of these references are based on quasi-static methods and in many cases only idealized structures are considered. In this section we will extend our formulation to take the effect of the dielectric anisotropy into account in addition to the effects of the metallization thickness and substrate mounting grooves.

For lossless anisotropic substrates, the permittivity tensor ϵ may be written in a diagonalized form [10]. Moreover, most of the substrates widely used in microwave integrated

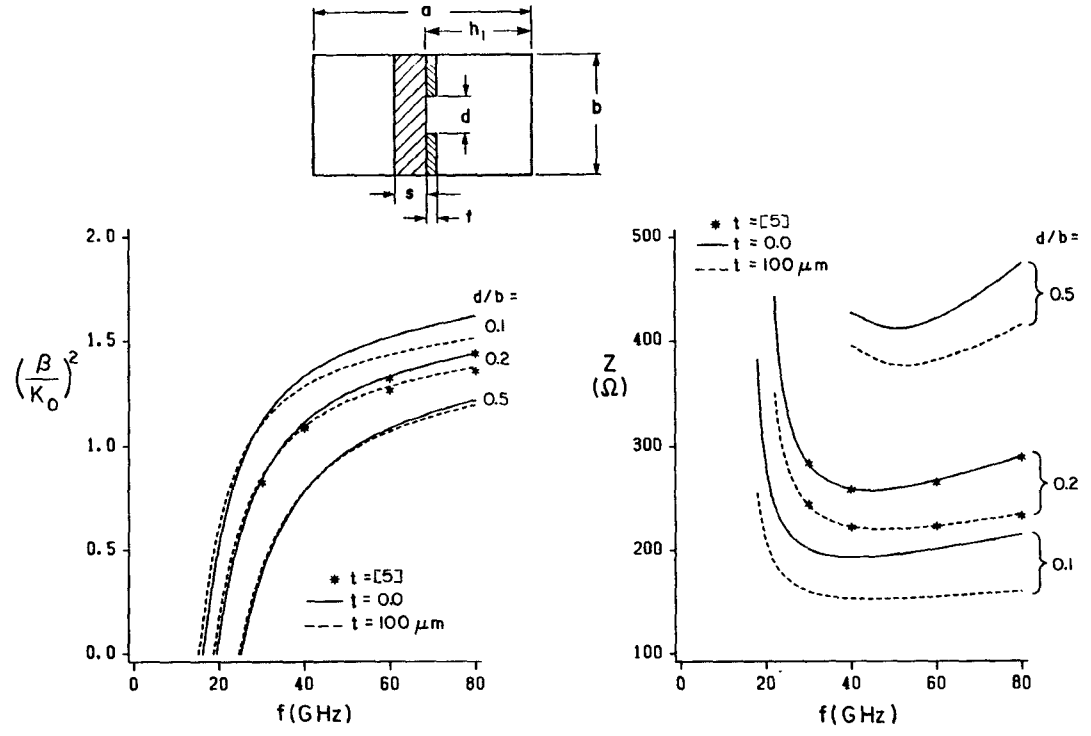

Fig. 4. Effective dielectric constant and characteristic impedance versus frequency in unilateral finlines with different values of slot width; $a = 2b = 4.7752$ mm, $S = 0.127$ mm, $h_1 = 2.3876$ mm, $\epsilon_r = 3.8$.

circuit design such as sapphire and Epsilam 10 are uniaxial crystals for which $\epsilon_{xx} = \epsilon_{zz}$. The permittivity tensor ϵ for this type of crystal can then be written as

$$\epsilon = \begin{bmatrix} \epsilon_2 & 0 & 0 \\ 0 & \epsilon_1 & 0 \\ 0 & 0 & \epsilon_2 \end{bmatrix}. \tag{23}$$

With the optic axis parallel to the y axis, the electric field of LSE modes will lie in the plane where no anisotropic effect is present. The solution in this case is basically the same as in the case of an isotropic medium with a dielectric permittivity ϵ_2. However, for LSM modes the situation is different because there is a component of the electric field in the y direction. In view of [10], the solution for LSM modes may be derived from

$$\begin{aligned} \vec{\prod}_n^e &= \Psi_n^e(x) e^{-j\alpha_n^e y} e^{-j\beta z} \vec{a}_y \\ \vec{h}_n^e &= j\omega\epsilon_2 \nabla \times \vec{\prod}_n^e \\ \vec{e}_n^e &= \omega^2 \mu \epsilon_2 \vec{\prod}_n^e + \nabla \nabla \cdot \vec{\prod}_n^e \end{aligned} \tag{24}$$

where Ψ_n^e is the solution of

$$\frac{\partial^2}{\partial x^2}\Psi_n^e(x) + \left[\omega^2\mu\epsilon_1 - \frac{\epsilon_1}{\epsilon_2}(\alpha_n^e)^2 - \beta^2\right]\Psi_n^e(x) = 0. \tag{25}$$

It can be readily shown that the transverse components of the fields in this case have the same form as those given in (3). However, α_n^h, α_n^e, Y_n^h, and Y_n^e are modified, becoming

$$\alpha_n^h = \left[\omega^2\mu\epsilon_2 - \left(\frac{n\pi}{L}\right)^2 - \beta^2\right]^{1/2} \tag{26}$$

$$\alpha_n^e = \left[\frac{\epsilon_2}{\epsilon_1}\right]^{1/2}\left[\omega^2\mu\epsilon_1 - \left(\frac{n\pi}{L}\right)^2 - \beta^2\right]^{1/2} \tag{27}$$

$$Y_n^h = \frac{\alpha_n^h}{\omega\mu} \qquad Y_n^e = \frac{\omega\epsilon_2}{\alpha_n^e}. \tag{28}$$

Thus, only a few minor changes are to be made in order to take the dielectric anisotropy into account. This illustrates the versatility of this approach and indicates how flexible and simple it is in dealing with complicated structures.

V. Numerical Results and Discussion

In Fig. 4 we show the effective dielectric constant $\epsilon_{\text{eff}} = (\beta/k_0)^2$ and the characteristic impedance Z versus frequency for unilateral finlines with different slot widths and for metallizations of $t = 0$ and $t = 100$ μm. Our results are in good agreement with those obtained by Kitazawa and Mittra [5], and our analysis can be used even for structures with infinitely thin fins. The results indicate that the metallization thickness has a significant effect on the characteristic impedance. Its effect, however, on the effective dielectric constant depends strongly on the slot width and is more pronounced for small slot widths.

To demonstrate the effect of the substrate mounting groove, Fig. 5 shows the normalized propagation constant of the dominant and the first higher order odd mode for groove depths of $e = 0$ and $e = 0.5$ mm. It is observed that

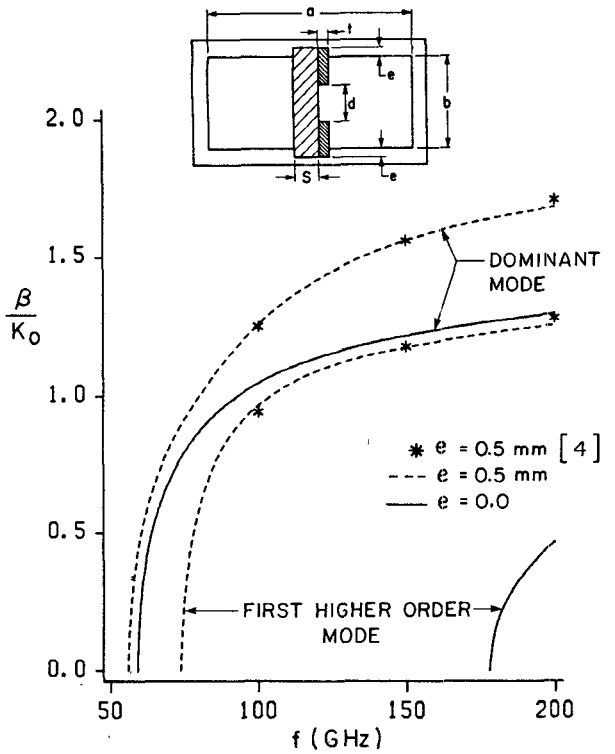

Fig. 5. Propagation characteristics of the dominant mode and first higher odd mode in a unilateral finline for $e = 0$ and $e = 0.5$ mm; $a = 2b = 1.65$ mm, $S = 0.11$ mm, $d = 0.3$ mm, $\epsilon_r = 3.75$, $t = 5$ μm.

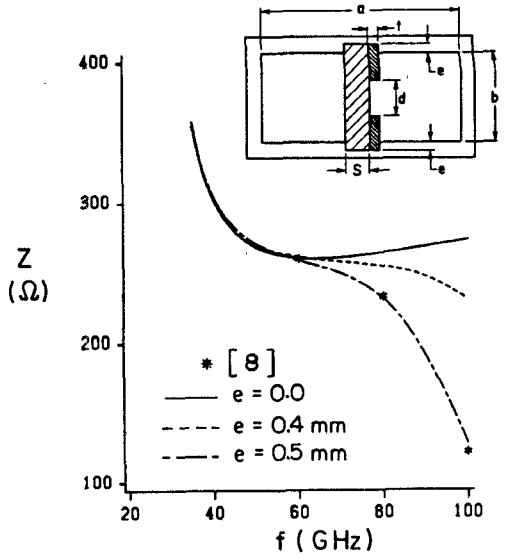

Fig. 6. Characteristic impedance of a unilateral finline versus frequency for different values of groove depth; $a = 2b = 3.1$ mm, $S = 0.22$ mm, $d = 0.4$ mm, $\epsilon_r = 3.75$, $t = 5$ μm.

neglecting the mounting groove leads to a higher cutoff frequency and a lower value for the propagation constant. This in fact is expected and is attributed to the part of the dielectric slab neglected in the mounting groove in the "ideal" case of $e = 0$. However, the effect of the groove on the dominant mode is significant when the first higher order mode starts to propagate. In addition, unlike the dominant mode's cutoff frequency, that of the first higher order mode decreases significantly when the mounting groove is used, leading to a very large reduction in the single-mode bandwidth.

Fig. 6 illustrates the effect of the mounting groove on the characteristic impedance. Our results confirm those recently published by Bornemann and Arndt [8]; the impedance follows the behavior of the dominant mode and starts to deviate from the ideal case ($e = 0$) only when the first higher order mode starts to propagate. In Fig. 7 we also show the effect of the metallization thickness on the single-mode bandwidth. It is observed that increasing the metallization thickness leads to a slight increase in the single-mode bandwidth and again the effect is more pronounced for smaller slot widths.

To demonstrate the fast convergence of the proposed analysis, Table I shows numerical results obtained for the propagation constant of the dominant and the first higher order modes and the characteristic impedance for a unilateral finline structure using different matrix sizes for the eignevalue equation. A matrix size of (6×6) is quite enough to provide convergent results within 0.5 percent.

It should be noted that the results given in Table I were obtained using (25 LSE modes+25 LSM modes) in the large guide; the number of modes retained in the slot was varied from (2 LSE modes+2 LSM modes) to (5 LSE modes+5 LSM modes). Although these results were obtained with $P/Q > b/d$, as has been shown in [9], in dealing with cascaded discontinuities the effect of the relative convergence problem becomes noticeable when $P/Q < R$ (in this case $R = b/d$), and as long as $P/Q \geq R$ good results can be achieved. It should be also mentioned that using a large number of modes in the large guide does not require a considerable computation effort since the sizes of the transmission matrices are determined by the number of modes retained in the slot [9]. The extra computation effort is involved in evaluating the matrix multiplication $[\boldsymbol{H}^{\dagger}\boldsymbol{P}_A^{\dagger}\boldsymbol{H}]$.

In Fig. 8 we show the frequency dependence of the effect of the metallization thickness on the dominant and the first higher odd mode and characteristic impedance in bilateral finlines. The results show that unilateral and bilateral finlines have identical behavior as far as the effect of the metallization thickness is concerned. A comparison is also given in this figure between our results and those published by Schmidt and Itoh [13] using the spectral-domain technique, and good agreement is observed for both the propagation constant and the characteristic impedance.

Fig. 9 illustrates the effect of the metallization thickness on the normalized propagation constant and characteristic impedance of the basic even and odd modes in coplanar lines. The metallization thickness has a negligible effect on the propagation characteristic of the odd mode over most of the operating range. Its effect, however, on the propagation of the even mode is significant over the whole range. Increasing the metallization thickness lowers the characteristic impedance in both cases.

Fig. 10(a) shows the effect of the mounting groove on the propagation characteristic of the dominant and first higher odd modes in coplanar lines where, again, behavior

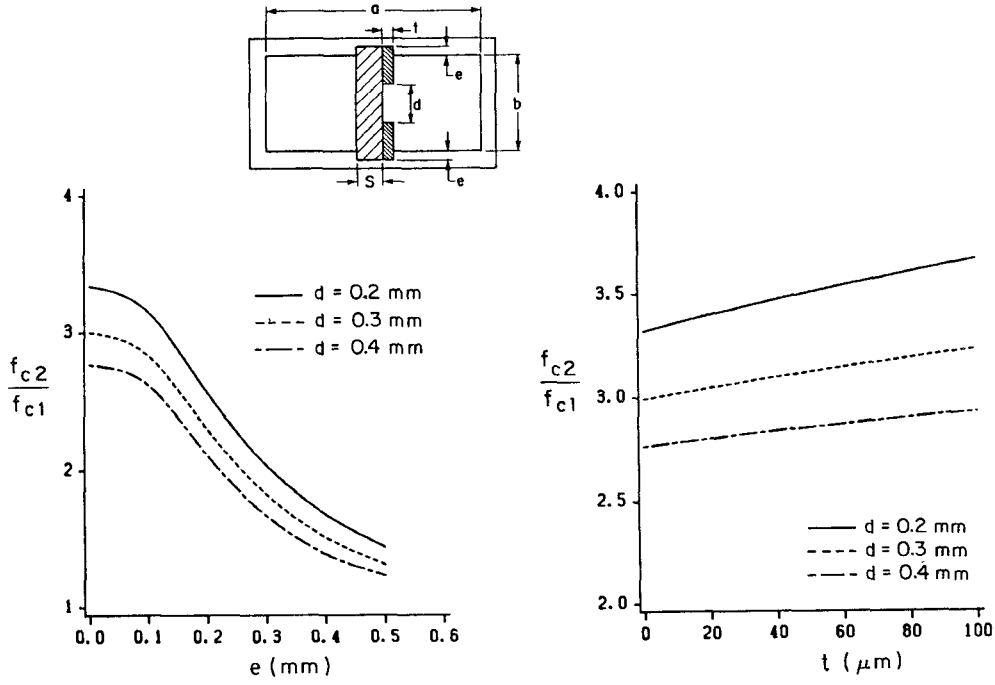

Fig. 7. Effects of the mounting groove depth and metallization thickness on the ratio f_{c2}/f_{c1}; $a = 2b = 1.65$ mm, $S = 0.11$ mm, $d = 0.3$ mm, $\epsilon_r = 3.75$. (a) $t = 5$ μm. (b) $e = 0$.

TABLE 1
THE NORMALIZED PROPAGATION CONSTANT AND CHARACTERISTIC IMPEDANCE OF A UNILATERAL FINLINE COMPUTED USING DIFFERENT MATRIX SIZES FOR THE EIGENVALUE EQUATION

Dominant Mode, f = 60 GHz

Matrix Size	β/K_0	Impedance (Ω)
(4x4)	1.1855	257.03
(6x6)	1.1866	258.75
(8x8)	1.1866	260.10
(10x10)	1.1854	260.83

First Higher Order Mode, f = 100 GHz

Matrix Size	β/K_0
(4x4)	0.36959
(6x6)	0.36911
(8x8)	0.36879
(10x10)	0.36851

$a = 2b = 3.1$ mm, $d = 0.4$ mm, $S = 0.22$ mm, $t = 5$ μm, $\epsilon_r = 3.75$.

similar to the unilateral finline is observed. The dispersion characteristics of coplanar lines with two dielectric layers are given in Fig. 10(b). A comparison between (a) and (b) in Fig. 10 shows that adding another dielectric layer may not enhance or compensate for the effect of the mounting groove.

In Fig. 11 the effect of the metallization thickness on the first four propagating modes in suspended microstrip lines is investigated. A noticeable effect is only observed on the propagation characteristic of the dominant mode, and our results agree well with those reported in [14] and [15]. Finally, we consider in Fig. 12 the effect of the metallization thickness on the normalized propagation constant in a coplanar line on sapphire substrate ($\epsilon_1 = 11.6, \epsilon_2 = 9.4$). We also compare our results with those given in [16] for unshielded coplanar lines. Our results are obtained for the shielded structure shown in Fig. 12 with electric walls at $\pm b/2$ for the even mode and with magnetic walls at $\pm b/2$ for the odd mode. A good agreement is observed between the results for the dominant even mode. The reason, however, for the discrepancy between the results of the odd mode at low frequencies is that for this mode the fields are not tightly bound to the slots, and the waveguide walls may not be far enough from the slots at low frequencies to simulate the open structure.

VI. CONCLUSIONS

The numerical results presented in this paper and the comparisons given with the other published data confirm the validity of the proposed analysis and show its simplicity in treating different planar structures with complicated configurations. With a reasonably small matrix size, the achievable accuracy of the solution exceeds most engineering requirements. The analysis can be extended to characterize planar transmission lines on semiconductor substrates. This also can be easily achieved since the dielectric layers are treated separately in the formulation. Thus, this approach promises to be useful as well in the design of monolithic microwave integrated circuits (MMIC's).

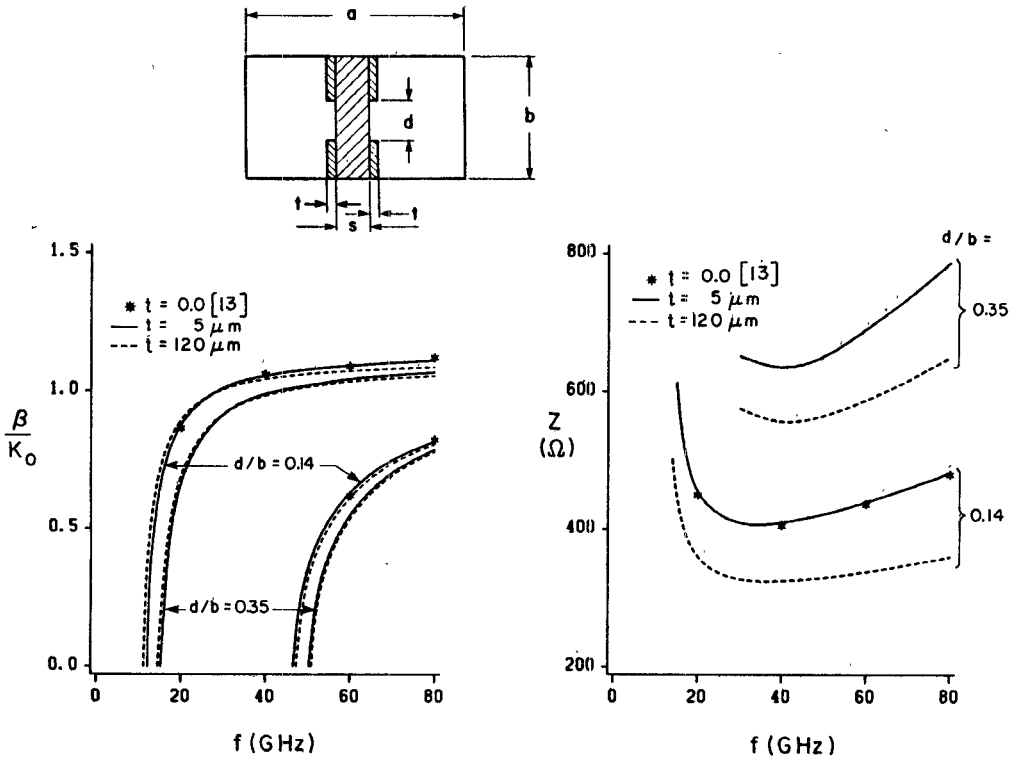

Fig. 8. Normalized propagation constant and characteristic impedance versus frequency in bilateral finlines; $a = 2b = 7.112$ mm, $S = 0.125$ mm, $\epsilon_r = 3$.

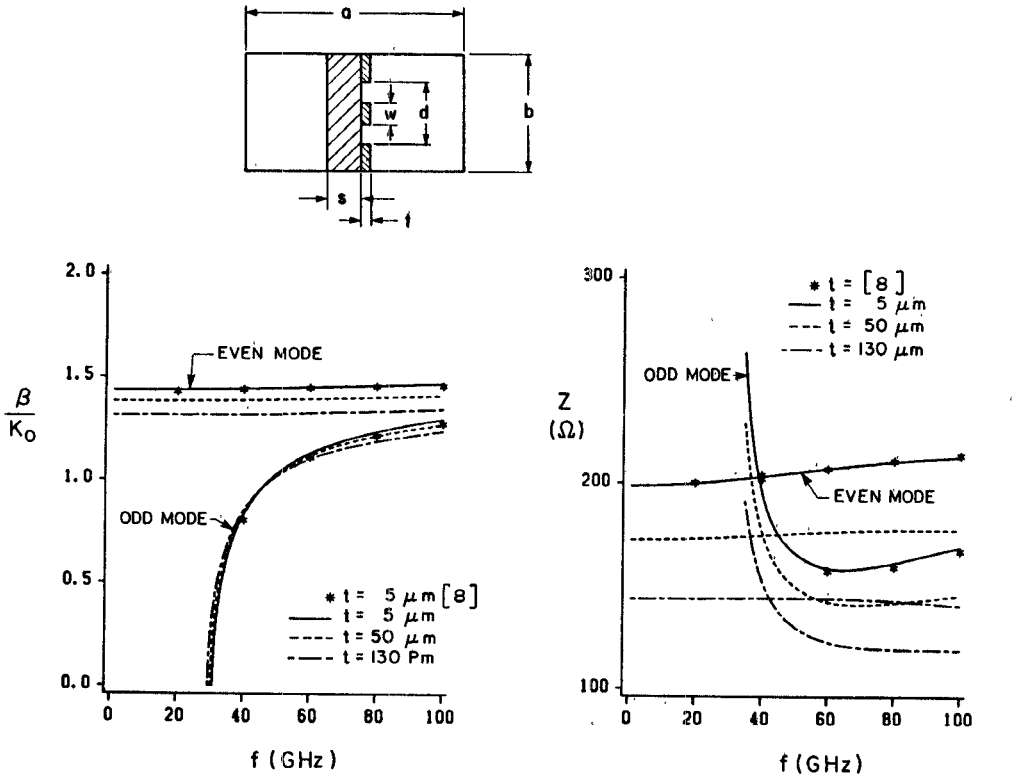

Fig. 9. Normalized propagation constant and characteristic impedance versus frequency in coplanar lines; $a = 2b = 3.1$ mm, $S = 0.22$ mm, $d = 0.6$ mm, $w = 0.2$ mm, $\epsilon_r = 3.75$.

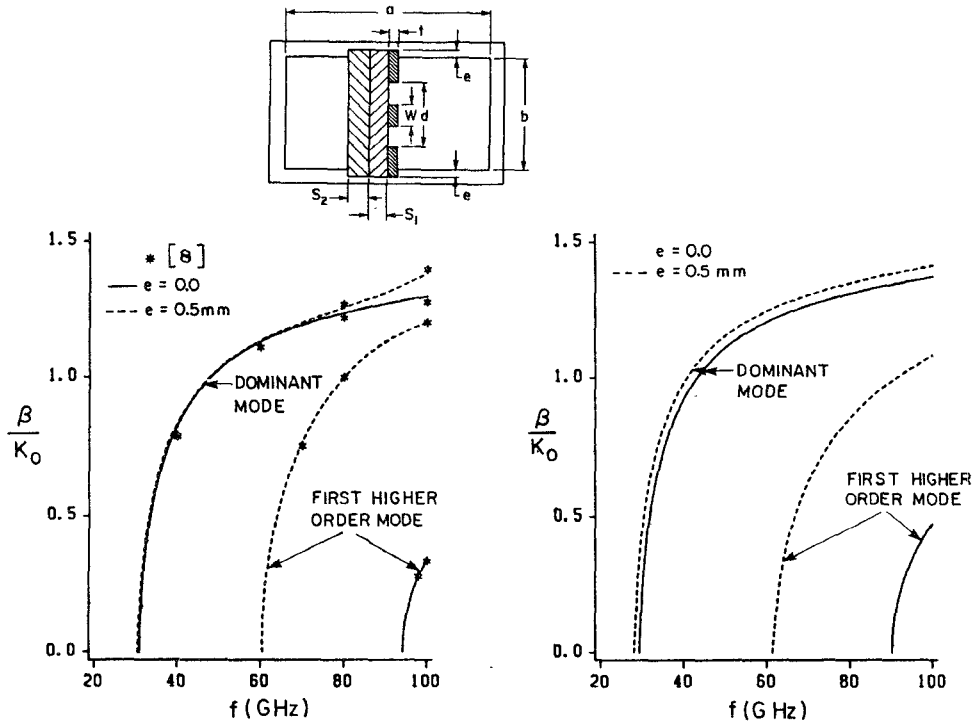

Fig. 10. Propagation characteristics of the dominant odd mode and first higher odd mode in a coplanar line for $e = 0$ and $e = 0.5$ mm; $a = 2b = 3.1$ mm, $S_1 = 0.22$ mm, $S_2 = 0.254$ mm, $d = 0.6$ mm, $w = 0.2$ mm, $t = 5$ μm. (a) $\epsilon_{r1} = 3.75, \epsilon_{r2} = 1.0$. (b) $\epsilon_{r1} = 3.75, \epsilon_{r2} = 2.2$.

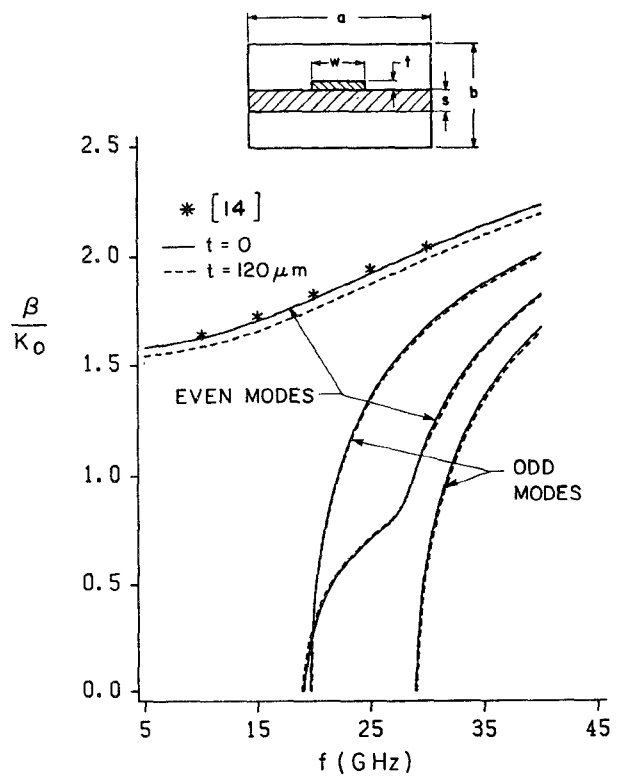

Fig 11 Normalized propagation constant as a function of frequency for the suspended microstrip line; $a = 2b = 7.112$ mm, $S = 0.635$ mm, $w = 1.0$ mm, $\epsilon_r = 9.6$.

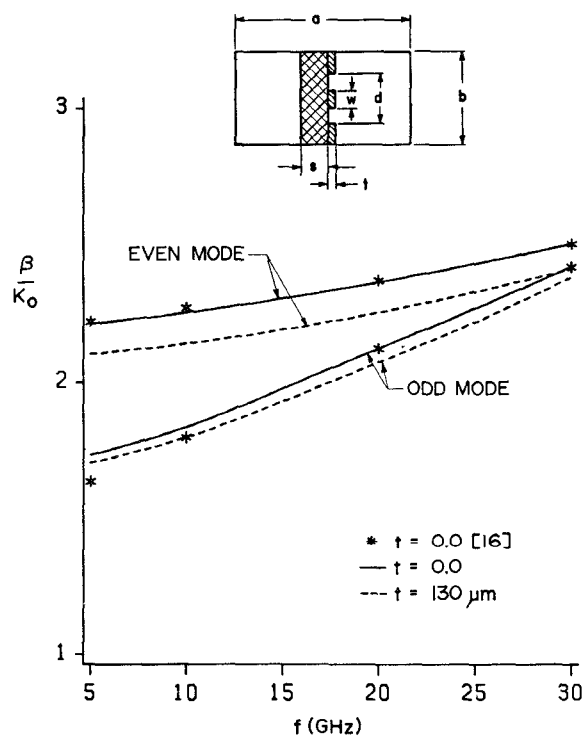

Fig. 12 Normalized propagation constant of a coplanar line of sapphire substrate; $a = 2b = 20$ mm, $S = 1.0$ mm, $d = 2.5$ mm, $w = 0.5$ mm, even mode (magnetic wall symmetry), odd mode (electric wall symmetry).

REFERENCES

[1] L. P. Schmidt, T. Itoh, and H. Hofmann, "Characteristics of unilateral finline structure with arbitrarily located slots," *IEEE Trans. Microwave Theory Tech.*, vol. MTT-29, pp. 352–355, Apr. 1981.

[2] A. S. Omar and S. Schunemann, "Formulation of the singular integral equation technique for planar transmission lines," *IEEE Trans. Microwave Theory Tech.*, vol. MTT-33, pp. 1313–1322, Dec. 1985.

[3] A. Beyer, "Analysis of the characteristics of an earthed fin line," *IEEE Trans. Microwave Theory Tech.*, vol. MTT-29, pp. 676–680, July 1981.

[4] R. Vahldieck, "Accurate hybrid-mode analysis of various finline configurations including multilayered dielectrics, finite metallization thickness and substrate holding grooves," *IEEE Trans. Microwave Theory Tech.*, vol. MTT-32, pp. 1454–1460, Nov. 1984.

[5] T. Kitazawa and R. Mittra, "Analysis of finlines with finite metallization thickness," *IEEE Trans. Microwave Theory Tech.*, vol. MTT-32, pp. 1484–1487, Nov. 1984.

[6] A. M. K. Saad and K. Schunemann, "Efficient eigenmode analysis for planar transmission lines," *IEEE Trans. Microwave Theory Tech.*, vol. MTT-30, pp. 2125–2131, Dec. 1982.

[7] R. Vahldieck and J. Bornemann, "A modified mode matching technique and its application to a class of quasi-planar transmission lines," *IEEE Trans. Microwave Theory Tech.*, vol. MTT-33, pp. 916–926, Oct. 1985.

[8] J. Bornemann and F. Arndt, "Calculating the characteristic impedance of finlines by transverse resonance method," *IEEE Trans. Microwave Theory Tech.*, vol. MTT-34, pp. 85–92, Jan. 1986.

[9] R. R. Mansour and R. H. MacPhie, "An improved transmission matrix formulation of cascaded discontinuities and its application to *E*-plane circuits," *IEEE Trans. Microwave Theory Tech.*, vol. MTT-34, pp. 1490–1498, Dec. 1986.

[10] R. Collin, *Field Theory of Guided Waves*. New York: McGraw-Hill, 1960.

[11] R. R. Mansour and R. H. MacPhie, "Scattering at an *N*-furcated parallel-plate waveguide junction," *IEEE Trans. Microwave Theory Tech.*, vol. MTT-33, pp. 830–835, Sept. 1985.

[12] N. G. Alexopoulos, "Integrated-circuit structures on anisotropic substrates," *IEEE Trans. Microwave Theory Tech.*, vol. MTT-33, pp. 847–881, Oct. 1985.

[13] L. P. Schmidt and T. Itoh, "Spectral domain analysis of dominant and higher order modes in fin-lines," *IEEE Trans. Microwave Theory Tech.*, vol. MTT-28, pp. 981–985, Sept. 1980.

[14] H. Hofmann, "Dispersion of planar waveguides for millimeter-wave applications," *Arch. Elek. Übertragung.*, Bd. 31, I, pp. 40–44, 1977.

[15] J. Bornemann, "Rigorous field theory analysis of quasiplanar waveguides," *Proc. Inst. Elec. Eng.*, vol. 132 pt. H. no. 1, pp. 1–6, Feb. 1985.

[16] T. Kitazawa and Y. Hayashi, "Coupled slots on an anisotropic sapphire substrate," *IEEE Trans. Microwave Theory Tech.*, vol. MTT-29, pp. 1035–1040, Oct. 1981.

✠

Raafat R. Mansour (S'84–M'86) was born in Cairo, Egypt, on March 31, 1955. He received the B.Sc (with honors) and M.Sc degrees from Ain Shams University, Cairo, in 1977 and 1981, respectively, and the Ph.D. degree from the University of Waterloo, Ontario, Canada, in 1986, all in electrical engineering.

He was a research fellow at the Laboratoire d'Electromagnetisme, Institut National Polytechnique, Grenoble, France, in 1981. From 1983 to 1986 he was a Research and Teaching Assistant with the Department of Electrical Engineering, University of Waterloo. Since then he has been with COM DEV Ltd., Cambridge, Ontario, as an advanced member of the technical staff. His present research interests are in the analysis and design of microwave and millimeter-wave integrated circuits.

Dr. Mansour has been awarded a Natural Sciences and Engineering Research Council of Canada NSERC fellowship in 1987.

✠

Robert H. MacPhie (S'57–M'63–SM'79) was born in Weston, Ontario, Canada, on September 20, 1934. He received the B.A.Sc. degree in electrical engineering from the University of Toronto in 1957 and the M.S. and Ph.D. degrees from the University of Illinois, Urbana, in 1959 and 1963, respectively.

In 1963, he joined the University of Waterloo, Waterloo, Ontario, Canada, as an Assistant Professor in Electrical Engineering and at present he is Professor of Electrical Engineering at Waterloo. His research interests currently focus on dipole antennas, waveguide scattering theory, scattering from prolate spheroid systems, and microstrip structures. During 1984–1985 he was on sabbatical leave as a Professeur Associé at the Université de Provence, France, working in the Département de Radioélectricité.